PHYSICAL REVIEW B VOLUME 22, NUMBER 11 1 DECEMBER 1980

Dynamic polarization echoes in metallic powders

F. Tsuruoka* and K. Kajimura
Electrotechnical Laboratory, Sakuramura, Ibaraki 305, Japan

(Received 2 June 1980)

Dynamic polarization echoes in normal and superconducting metal powders have been investigated. The dynamic echoes are found to be caused by the anharmonicity of the mechanical oscillators excited by rf fields in static magnetic fields, but not by the parametric coupling of the applied rf fields to the oscillator modes. Most of the experimental data showed a large signal effect even at the lowest applied pulse amplitudes consistent with adequate signal to noise. Effects of rf pulse interval and amplitudes, static magnetic field, temperature, and the angle between rf and static magnetic fields, ψ, on the echo amplitude are consistently explained by the calculation in the large signal regime, where the higher-order interactions between anharmonically oscillating modes are effective. Dependence of the echo amplitude on the angle ψ revealed that the mechanical oscillation consists of different oscillation modes. The damping constant of the two pulse echo affected by surrounding media, rf frequency, static magnetic field, and temperature is well understood based upon the energy transmission from an individual oscillating particle to the media and internal loss such as energy absorption due to conduction electrons, thermal phonons, and crystalline imperfections.

I. INTRODUCTION

Polarization echoes refer to the coherent pulsed fields emitted at $t = 2\tau$ and $T + \tau$ from materials after three pulsed rf fields applied at $t = 0$, τ, and T. Polarization echoes have been observed in a wide variety of powders and bulk materials. Dynamic and static polarization echoes of piezoelectric powders have been extensively studied both experimentally and theoretically.[1] Dynamic echoes possess relaxation times which are associated with inherent dynamic behavior of the particles. The term static echoes refers to the echo phenomena in which the relaxation time of the stimulated three pulse echo exceeds the lifetime of any dynamic processes.

According to Gould[2] all echo phenomena are separated into two classes depending on the type of nonlinear mechanism responsible for echo formation in a classical oscillator system. Parametric field-mode interactions are those in which the applied field couples parametrically to the previously excited modes of the system causing phase reversal and subsequent echo formation. In anharmonic oscillator systems the different free oscillation modes are coupled anharmonically even though the oscillator systems interact linearly with the applied field. The two classes can be clearly distinguished experimentally.[1,3] In the case of parametric field-mode interaction systems echoes decay monotonically from a finite value with increasing two-pulse separation τ, whereas in the anharmonic oscillator systems echoes build up from zero at $\tau = 0$ and go through a maximum before decreasing exponentially at large τ.

Metallic powder echoes similar to nuclear-spin echoes have been known since 1966.[4] Since the experimental procedure of the polarization echoes in metallic powders is much similar to that of spin echoes, the polarization echoes of the metallic powders have been found during the course of the spin-echo study. The polarization echoes are distinguished from nuclear-spin echoes through no relation between the strength of the static magnetic field and the carrier frequency.

We use the pulse sequence shown in Fig. 1 throughout this paper. The rf magnetic field pulses with the carrier frequency ω_0, peak amplitudes B_1, B_2, and B_3, and widths Δ_1, Δ_2, and Δ_3 are applied to the powders placed in a static magnetic field B_0 at times $t = 0$, τ, and T, respectively. At the times $t = m\tau$ ($m = 2, 3, 4, \ldots$) the powders coherently radiate the two-pulse echoes $e_2(m\tau)$. At the times $t = T + p\tau$ ($p = 1, 2, 3, \ldots$) the powders coherently radiate the three-pulse echoes $e_3(T + p\tau)$. For sufficiently large τ the two-pulse echo $e_2(2\tau)$ decays exponentially as $e_2(2\tau) \sim \exp(-2\tau/T_2)$, where T_2 is a phenomenological decay time constant. The decay time T_2 is associated with the mechanical damping of the individual powder particles, the origin of which should be discussed separately. The three-pulse echo $e_3(T + \tau)$ decays as $\exp(-T/T_1)$. The relaxation time T_1 is equal to $\frac{1}{2}T_2$ for dynamic echoes considered here.

Goldberg *et al.*[5] observed echoes from type-II superconducting powders, VTi and NbZr, which are not explained by the spin-echo mechanism. Alloul and Froidevaux[6,7] and later Snodgrass[8] noted that the echo properties of normal metal powders were quite similar to those reported by Goldberg *et al.*[5] Alloul

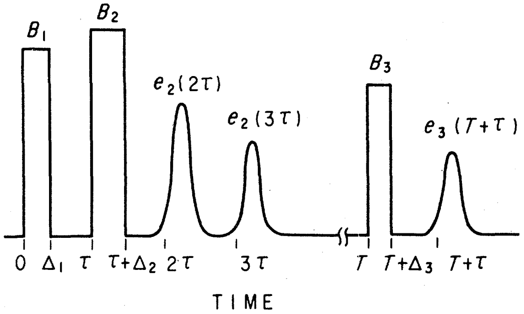

FIG. 1. Schematic pulse timing for a three-pulse sequence. The pulses and signals all have a common rf carrier frequency ω_0.

and Froidevaux[7] pointed out that the echoes were associated with magnetoacoustic oscillations. Ehrenfreund *et al.*[9] proposed a model which partially accounted for the experimental dependence of the echo amplitude on rf pulse amplitudes in Ref. 5 without specifying the origin of the nonlinearity responsible for the echoes. Pacult *et al.*[10] discussed the origin of echoes from three different points of view: (i) helicon waves; (ii) microscopic acoustic vibrations within individual particles; and (iii) macroscopic mechanical vibrations of the whole powder. They pointed out that their experimental result on pure and alloy metallic powders was in favor of (iii). Kupca and Searle[11] have carried out a rather detailed experiment on normal and ferromagnetic metal powders bearing in mind that the echoes are due to the excitation and subsequent rephasing of elastic vibrational modes of the particles. However, they did not come to a definite conclusion as to the nonlinearity responsible for the echo formation, since the rf and static magnetic field dependence was too complex to be described by a simple form expected from a simple theoretical model. We shall show later that the deviation from a simple relationship is due to the effect of higher-order terms of the interaction between anharmonic oscillators. Theoretical investigation has been recently carried out by Vodop'yanov *et al.*[12] who treated the system as an electromagnetically excited anharmonic oscillator system and compared their result with the experiment of Ref. 11. In their calculation, however, they missed the buildup term, which is an evidence for the anharmonic oscillator mechanism, and also the role of the static magnetic field in the electromagnetic detection of the echoes.

In this paper we present a detailed experimental study of the dynamic polarization echoes in normal metallic Al, Sn, Nb, and Cu, and type-II superconducting V_3Si powders. Although we found static echoes in these metallic powders,[13] we shall discuss only dynamic echoes here. The static echoes in the metallic powders will be discussed separately. One of the main conclusions of this paper is that the metallic powder echoes are well explained by the anharmonic oscillator model. In Sec. II we present a calculation of the electromagnetic excitation of mechanical oscillators in a metallic particle acting as an acoustic resonator and the formation of dynamic polarization echoes via lattice anharmonicity. In Sec. III experimental procedures are described. In Sec. IV experimental results are discussed in the light of the calculation given in Sec. II. A summary of the results and conclusions is presented in Sec. V.

II. THEORY

A. Linear excitation and detection of mechanical oscillation in metals

Since the linear excitation of acoustic oscillations at a metal surface has been well investigated,[14] we describe briefly the excitation mechanism and apply the argument to the excitation and detection of the oscillation in a single metallic particle with simple geometries in order to discuss later the echo formation mechanism in a large number of particles.

1. Excitation at metal surface

Acoustic oscillations in metals in static magnetic field, $\vec{B}_0$, are excited by rf magnetic field $\vec{B}(t)$. The shielding current is induced at the surface within a skin depth by the rf field. Transverse- or longitudinal-acoustic waves can be produced depending on the orientation of $\vec{B}_0$ relative to the surface shielding current. In order to have the idea of the transverse and longitudinal forces acting on the lattice ions we assume that the metal occupies the half space $z \geqslant 0$ and the direction of $\vec{B}(t)$ is parallel to the metal surface. For $\vec{B}_0$ along x, the Lorentz force acting on the electrons is along z, resulting in a variation of the electron charge density along z. An internal electric field along z is set up to maintain local charge neutrality and provides the driving force for the longitudinal waves. On the other hand, when $\vec{B}_0$ is along z, the shielding current induced by $\vec{B}(t)$ is acted on by the Lorentz force in the x direction. Since the electrons and ions composing the shielding current move in the opposite directions and have opposite charges, the Lorentz forces on them act in the same direction to produce a coherent driving force for the transverse-acoustic waves. In type-II superconductors the acoustic waves are excited in the same manner as in normal metals when the static magnetic field is much greater than the lower critical field of the superconductors. In order to describe the ionic displacement field $\vec{\xi}(z,t) \sim \exp[i(\omega_0 t - qz)]$ (angular frequency ω_0 and wave vector $\vec{q}$ along z) resulting from the response of the metal to the disturbance $\vec{j}_0$

which is the shielding current induced by $\vec{B}(t)$, we need the relation between the currents and the electric fields inside the metal and the equation of motion of the lattice ions in the electric and magnetic fields. From the Fourier transforms of the Maxwell equations[15] we have the relation between the total current $\vec{J}(\vec{q})$ and the electric field $\vec{E}(\vec{q})$:

$$\vec{J}(\vec{q})=\overleftrightarrow{\Gamma}\vec{E}(\vec{q}) \ , \tag{1a}$$

where the tensor $\overleftrightarrow{\Gamma}$ is given by

$$\overleftrightarrow{\Gamma}=\mathrm{diag}(i\beta\sigma_0,\ i\beta\sigma_0,\ -i\omega_0/4\pi) \ . \tag{1b}$$

Here, σ_0 is the static electronic conductivity and

$$\beta=(c^2q^2/4\pi\sigma_0\omega_0)(1-\omega_0^2/c^2q^2) \ . \tag{1c}$$

The total current is the sum of the ionic $\vec{j}_i = n_0e(\partial\vec{\xi}/\partial t)$, the electronic $\vec{j}_e$, and the shielding currents $\vec{j}_0$:

$$\vec{J}=n_0e\frac{\partial\vec{\xi}}{\partial t}+\vec{j}_e+\vec{j}_0 \ , \tag{2a}$$

where n_0 is the number density of conduction electrons and $-e$ is the electronic charge. Cohen *et al.*[16] showed that the electronic current is given by

$$\vec{j}_e(\vec{q})=\overleftrightarrow{\sigma}(\vec{q},\omega_0)\left(\vec{E}(\vec{q})-\frac{m}{e\tilde{\tau}}\frac{\partial\vec{\xi}(\vec{q})}{\partial t}\right) + n_0e\overleftrightarrow{D}\vec{q}[\vec{q}\cdot\vec{\xi}(\vec{q})] \ , \tag{2b}$$

where $\overleftrightarrow{\sigma}(\vec{q},\omega_0)$ is the magnetoconductivity tensor, $\tilde{\tau}$ is the electronic relaxation time, and

$$\overleftrightarrow{D}=[2E_F/3n_0e^2(1+i\omega_0\tilde{\tau})]\overleftrightarrow{\sigma}(\vec{q},\omega_0) \tag{2c}$$

is the diffusion tensor, E_F being the Fermi energy. The equation of motion of the lattice ions in elastically isotropic metals is given by[15]

$$M\frac{\partial^2\vec{\xi}}{\partial t^2}+2\Gamma_0M\frac{\partial\vec{\xi}}{\partial t}=C_l\vec{\nabla}(\vec{\nabla}\cdot\vec{\xi})-C_t\vec{\nabla}\times(\vec{\nabla}\times\vec{\xi})+Ze\vec{E}+\frac{Ze}{c}\frac{\partial\vec{\xi}}{\partial t}\times\vec{B}_0-\frac{Ze}{\sigma_0}\vec{j}_e-\frac{Zn_0e^2}{\sigma_0}\frac{\partial\vec{\xi}}{\partial t} \ , \tag{3}$$

where M is the ionic mass, Γ_0 is the nonelectronic damping constant, C_l and C_t are elastic moduli for longitudinal and transverse waves, respectively, and Ze is the ionic charge. We can obtain general solutions to $\vec{\xi}$ in terms of $\vec{B}(t)$ from Eqs. (1a), (2a), and (3). However, it is much more informative to see the solutions for two representative geometries, $\vec{B}_0 \parallel \vec{q} \parallel z$ and $\vec{B}_0 \parallel x \perp \vec{q} \parallel z$, as shown by Meredith *et al.*[17] in the local limit, $ql < l$, where l is the electronic mean free path.

When $\vec{B}_0 \parallel \vec{q} \parallel z$, it can be shown that the transverse components of the incident electromagnetic wave are coupled only to the transverse ionic motions but not to the longitudinal motions. Writing the combined transverse components

$$E_\pm=E_x \pm iE_y \tag{4a}$$

and similarly for $B_\pm$, $J_\pm$, and $\xi_\pm$, and

$$\sigma_\pm=\sigma_{xx}\mp i\sigma_{xy} \ . \tag{4b}$$

We obtain, respectively, from Eqs. (1a), (2a), and (2b)

$$J_\pm(\vec{q})=i\beta\sigma_0E_\pm(\vec{q}) \ , \tag{5}$$

$$J_\pm(\vec{q})=i\omega_0n_0e\xi_\pm(\vec{q})+j_{e\pm}(\vec{q})+j_{0\pm}(\vec{q}) \ , \tag{6}$$

$$j_{e\pm}(\vec{q})=\sigma_\pm(\vec{q},\omega_0)[E_\pm(\vec{q})-(i\omega_0m/e\tilde{\tau})\xi_\pm(\vec{q})] \ , \tag{7}$$

since the diffusion current in Eq. (2b) is zero for the transverse displacement. The shielding current $j_{0\pm}(\vec{q})$ in Eq. (6) is related to the rf field, $B_\pm(t)$, at the metal surface, $z=+0$, by

$$j_{0\pm}(\vec{q})=\pm(ic/4\pi^2)B_\pm(t) \ . \tag{8}$$

Equation (3) becomes

$$(-\omega_0^2+2i\omega_0\Gamma+v_{t0}^2q^2\mp\Omega_c\omega_0+iZm\omega_0/M\tilde{\tau})\xi_\pm(\vec{q}) = (Ze/M)E_\pm(\vec{q})-(Ze/M\sigma_0)j_{e\pm}(\vec{q}) \ , \tag{9}$$

where $\Omega_c=(Zm/M)\omega_c$ is the ionic cyclotron frequency, $\omega_c=eB_0/mc$ being the electronic cyclotron frequency, $v_{t0}=\sqrt{C_t/M}$ is the unrenormalized velocity of transverse waves. The conductivity $\sigma_\pm(\vec{q},\omega_0)$ is given by

$$\sigma_\pm(\vec{q},\omega_0)=\sigma_0(1-\tfrac{1}{5}k^2)/[1+i(\omega_0\mp\omega_c)\tilde{\tau}] \ , \tag{10a}$$

$$k=-ql/[1+i(\omega_0\mp\omega_c)\tilde{\tau}] \ . \tag{10b}$$

By eliminating $J_\pm(\vec{q})$, $E_\pm(\vec{q})$, and $j_{e\pm}(\vec{q})$ from Eqs. (5)–(9), we obtain the transverse displacement $\xi_\pm(\vec{q})$ in terms of $B_\pm(t)$,

$$(-\omega_0^2+2i\omega_0\Gamma+v_t^2q^2)\xi_\pm(\vec{q})=-\frac{B_0B_\pm(t)}{4\pi^2\rho(1-i\beta)} \ , \tag{11a}$$

where

$$\Gamma=\Gamma_0+\Gamma_B \ , \tag{11b}$$

$$\Gamma_B=c^4\Omega_c^2\omega_0^2/8\pi v_t^4\Omega_p^2\sigma_0+n_0 m v_F^2\omega_0^2\tilde{\tau}/10\rho v_t^2 \ , \tag{11c}$$

$$v_t^2=v_{t0}^2[1+(\Omega_c^2c^2/\Omega_p^2v_{t0}^2)] \ , \tag{11d}$$

$p=n_0M/Z$ is the density of the metal, $\Omega_p=(Zm/M)^{1/2}\omega_p$ is the ionic plasma frequency, and $\omega_p=(4\pi n_0e^2/m)^{1/2}$ is the electronic plasma frequency. By making the inverse Fourier transform of Eq. (11a), we obtain the equation of motion for transverse displacement

$$\frac{\partial^2\xi}{\partial t^2}+2\Gamma\frac{\partial\xi}{\partial t}-v_t^2\frac{\partial^2\xi}{\partial z^2} =\frac{B_0B(t)}{4\pi\rho}\left[\frac{1+i}{\delta}\right]\exp\left[-\frac{(1+i)z}{\delta}\right] \ , \tag{12a}$$

where

$$\delta=c/\sqrt{2\pi\sigma_0\omega_0} \tag{12b}$$

is the classical skin depth. The right-hand side (rhs) of Eq. (12a) indicates the driving Lorentz force caused by the static magnetic field and the current induced by the rf magnetic field which penetrates to about the skin depth.

When $\vec{B}_0 \parallel x \perp \vec{q} \parallel z$, it follows from Eqs. (1a) and (2a) that the equation of motion of ions, Eq. (3), is written in the form

$$[\omega_0^2-2i\omega_0\Gamma_0-(v_l^2-v_t^2)\vec{q}\vec{q}-v_t^2q^2+i\omega_0\vec{\Omega}]\vec{\xi}(\vec{q})+\frac{Ze}{M}(1-\vec{\Gamma}/\sigma_0)\vec{E}(\vec{q})=-\frac{Ze}{M\sigma_0}\vec{j}_0(\vec{q}) \ . \tag{13}$$

Here, $v_l=\sqrt{C_l/M}$ is unrenormalized velocity of longitudinal waves, the tensor $\vec{\Omega}$ has yz component Ω_c and zy component $-\Omega_c$, and its other components are zero, and the dyadic $\vec{q}\vec{q}$ has zz component q^2 and all its other components are zero. It follows from Eqs. (1a), (2a), (2b), and (2c) that

$$(1-\vec{R}\cdot\vec{\Gamma})\vec{E}(\vec{q})=\left[-\frac{2E_F}{3e(1+i\omega_0\tilde{\tau})}\vec{q}\vec{q}+\frac{in_0e\omega_0}{\sigma_0}(1-\sigma_0\vec{R})\right]\vec{\xi}(\vec{q})-\vec{R}\cdot\vec{j}_0(\vec{q}) \ , \tag{14}$$

where $\vec{R}$ is a resistivity tensor defined as the inverse of the magnetoconductivity tensor, $\vec{\sigma}(\vec{q},\omega_0)$, introduced in Eq. (2b). The equation of motion of ions is given by eliminating $\vec{E}(\vec{q})$ from Eqs. (13) and (14). It can be shown that the driving force is along the z axis and ξ_x parallel to B_0 is not excited by the rf field in this geometry. When the static magnetic field is not so intense the acoustic wave produced by the rf field becomes nearly a pure longitudinal wave. The equation of motion for such a longitudinal displacement is given by

$$(-\omega_0^2+2i\omega_0\Gamma+v_lq^2)\xi_z=-\frac{B_0B(t)}{4\pi^2\rho(1-i\beta)} \ , \tag{15a}$$

where

$$\Gamma=\Gamma_0+\Gamma_B \ , \tag{15b}$$

$$\Gamma_B=c^4\Omega_0^2\omega_0^2/8\pi v_l^4\Omega_p^2\sigma_0+2n_0mv_F^2\omega_0^2\tilde{\tau}/15\rho v_l^2 \ , \tag{15c}$$

$$v_l^2=v_{l0}^2[1+(\Omega_c^2c^2/\Omega_p^2v_{l0}^2) + Zmv_F^2/3Mv_{l0}^2(1+\omega_0^2\tilde{\tau}^2)] \ . \tag{15d}$$

The inverse Fourier transform of Eq. (15a) becomes

$$\frac{\partial^2\xi}{\partial t^2}+2\Gamma\frac{\partial\xi}{\partial t}-v_l^2\frac{\partial^2\xi}{\partial z^2} =\frac{B_0B(t)}{4\pi\rho}\left[\frac{1+i}{\delta}\right]\exp\left[\frac{-(1+i)z}{\delta}\right] \ , \tag{16}$$

which has an identical form to Eq. (12a). The equations of motion of metallic ions, Eqs. (12a) and (16), are essentially the same as Eq. (3) of Ref. 1 except for the form of the driving force on the rhs of Eqs. (12a) and (16).

2. Application to a metal particle

We approximate an irregularly shaped metal particle by an elastically isotropic thin platelet of thickness $2d$ and cross-sectional area A. Other several cases of the particle geometry are mentioned at the end of this subsection. The orientation of the external rf field relative to the platelet surface is given by the angle θ and it is assumed that the parallel component of the rf field, $B(t)\cos\theta$, couples to the thickness vibrations of the platelet. We take the z axis normal to the platelet surface and the x axis in the direction of the projection of $\vec{B}(t)$ to the platelet surface. The

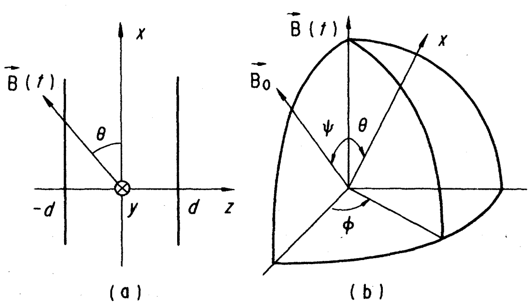

FIG. 2. (a) Rectangular Cartesian coordinate system for specifying the direction of the rf magnetic field relative to the platelet surfaces, $z=\pm d$. (b) Relative directions of the rf and static magnetic fields and the x axis.

orientation of the static magnetic field, $\vec{B}_0$, relative to the rf field and the x axis is specified by two angles ψ and ϕ as shown in Fig. 2. Then the parallel (x) and perpendicular (z) components of $\vec{B}_0$ to the platelet surface are expressed as

$$B_{0x} = B_0\Theta_x \ , \tag{17a}$$

$$\Theta_x = \sin\psi \sin\theta \cos\phi + \cos\psi \cos\theta \ , \tag{17b}$$

$$B_{0z} = B_0\Theta_z \ , \tag{17c}$$

$$\Theta_z = -\sin\psi \cos\theta \cos\phi + \cos\psi \sin\theta \ . \tag{17d}$$

On the basis of the argument in Sec. II A 1, we assume that the rf field parallel to the platelet surface and the z component of $\vec{B}_0$ produce the transverse displacement of ions of amplitude $\xi_x(z,t)$ and the x component of $\vec{B}_0$ selectively excites the longitudinal displacement, $\xi_z(z,t)$. Both faces of the platelet placed in an rf coil receive the same rf field $B(t)\cos\theta$, since the thickness of the platelet is assumed to be much shorter than the wavelength of the electromagnetic wave having the frequency ω_0. The shielding currents induced by the rf field are antisymmetric with respect to the plane $z=0$ of the platelet. It follows from Eq. (11a) that the equation of motion for both ξ_x and ξ_z is expressed by

$$\frac{\partial^2\xi}{\partial t^2} + 2\Gamma\frac{\partial\xi}{\partial t} - v^2\frac{\partial^2\xi}{\partial z^2} = \frac{B_0B(t)\Theta\cos\theta}{4\pi\rho}\,\frac{1+i}{\delta}\left[\exp\left(\frac{-(1+i)(z+d)}{\delta}\right) - \exp\left(\frac{(1+i)(z-d)}{\delta}\right)\right] \ . \tag{18}$$

Here, v and Θ denote v_t and Θ_z, respectively, for the transverse wave and v_l and Θ_x for the longitudinal wave. Following the procedure to solve the equation of motion in Ref. 1 we express the equation of motion with respect to a spatially normalized strain term $S(t)$ defined by

$$\xi(z,t) = m(z)S(t) \ , \tag{19a}$$

where $m(z)$ is a real, odd, normal-mode function normalized according to

$$V^{-1}\int m^2 dV = \tfrac{1}{2}d^2 b \ , \tag{19b}$$

V and b being the particle volume and a normalization constant. If we take $m(z)$ to be an odd simple function,

$$m(z) = d\,\sin qz \ , \tag{19c}$$

the normalization constant becomes

$$b = 1 - \sin(2qd)/2qd \ . \tag{19d}$$

Inserting Eq. (19a) into Eq. (18) we obtain

$$\frac{\partial^2 S}{\partial t^2} + 2\Gamma\frac{\partial S}{\partial t} + \Omega^2 S = \frac{\gamma B_0 B(t)\Theta\cos\theta}{4\pi\rho(1+\beta^2)^{1/2}} \ , \tag{20a}$$

where

$$\Omega^2 = -v^2\int m\frac{\partial^2 m}{\partial z^2}dV \Big/ \int m^2 dV \ , \tag{20b}$$

$$\gamma = -(2/d^2)e^{i\chi}\left[1 + \exp\left(-(1+i)\frac{2d}{\delta}\right)\right] \ , \tag{20c}$$

$$\chi = \tan^{-1}\beta \ . \tag{20d}$$

We take $B(t)$ to be the imaginary part of a rectangular rf pulse applied at $t=t_0$ with amplitude B and width Δ.

$$B(t) = Be^{i\omega_0(t-t_0)}[U(t-t_0) - U(t-t_0-\Delta)] \ , \tag{21}$$

where U is the unit step function. The solution of Eq. (20a) with the rf pulse [Eq. (21)] corresponding to the thickness resonance of the platelet is given by

$$S(t) = S(t_0) - \left(\frac{i\gamma B_0 B\Theta\cos\theta}{8\pi\rho\Omega\Gamma(1+\beta^2)^{1/2}}\right) \times e^{(-\Gamma+i\Omega)(t-t_0)}\left(\frac{e^{f\Gamma\Delta}-1}{f}\right) \ , \tag{22a}$$

where

$$f = 1 + i\omega/\Gamma \ , \tag{22b}$$

$$\omega = \omega_0 - \Omega \ . \tag{22c}$$

In deriving Eq. (22a) we used the approximation that the envelope of $S(t)$ slowly varies compared to Ω^{-1} and $\Omega/\Gamma >> 1$, and we neglected the sum frequency term in $\omega_0 + \Omega$.

Several cases of particle geometry other than a thin platelet have been also considered. We shall only mention here that for a metallic disc or sphere with a radius nearly matching to a quarter of a sound wavelength the equation of motion and its solution are expressed by equations similar to Eqs. (20a) and (22a), respectively.

3. Circuit response to particle oscillation

The oscillation of a metal particle in the static magnetic field, $\vec{B}_0$, is detected electromagnetically in an inductance coil. We consider first the detection of transverse waves arriving at the metal surfaces $z = \pm d$. By eliminating the total current density

$J_\pm(\vec{q})$ from Eqs. (5), (6), and (7) and writing $R_\pm = \sigma_\mp^{-1}(\vec{q}, \omega_0)$ we obtain

$$E_\pm(\vec{q}) = \frac{n_0 e}{\sigma_0} \frac{1-\sigma_0 R_\pm}{1-i\beta\sigma_0 R_\pm} \frac{\partial \xi_\pm(\vec{q})}{\partial t} \quad . \tag{23}$$

Here, we dropped $j_{0\pm}$ induced by the external rf field, $B_\pm(t)$, in Eq. (6), since we detect the oscillation without $B_\pm(t)$. The electric field at the metal surfaces, $z = \pm d$, is given by the inverse transform of Eq. (23) as

$$\vec{E}(\pm d,t) = -\frac{1}{c(1-i\beta)} \left(\frac{\partial \vec{\xi}(\pm d,t)}{\partial t} \times \vec{B}_0 \right) , \tag{24}$$

where we used the relation $\beta\omega_c\tau << 1$. For longitudinal waves, it can be shown easily using Eq. (13) that the electric field has the identical form to Eq. (24). Since the tangential component of the electric field is continuous at the boundary between the metal surface and free space, the rf magnetic field, $B_r(t)$, is radiated from the metal surface to the free space, which is detected by the coil. The total magnetic field radiated from the platelet is $2AB_r(t)$. The time derivative of the radiated rf magnetic field is related to the electric field at the metal surface by the Maxwell equation

$$\frac{\partial \vec{B}_r(t)}{\partial t} = -c\vec{\nabla} \times \vec{E}(\pm d,t) \quad . \tag{25}$$

The voltage response of a circuit containing a sample consisting of a large number of particles is given by the time derivative of the magnetic flux in the coil

$$V(t) = \sum_\omega v_\omega = \sum_\omega 2aA \frac{\partial \vec{B}_r(t)}{\partial t} \cdot \hat{e} G_R(\omega) \quad , \tag{26}$$

where ω is the difference frequency defined in Eq. (22c) which is used here as a particle mode label, the sum $\sum_\omega$ is over all modes of all particles, a is the factor coming from the coil geometry, $\hat{e}$ is the unit vector in the direction of the coil axis relative to the radiation surface, and $G_R(\omega)$ is the rf frequency response of the circuit and voltage receiver. In the limit of an infinite number of modes, the sum in Eq. (26) can be replaced by a double integral over the mode distribution $D(\omega)$ and the solid angle $\sin\theta d\theta d\phi$. Taking the distribution of particle orientations to be uniform we find

$$\sum_\omega v_\omega \to \frac{1}{4\pi} \int_0^{2\pi} d\phi \int_0^\pi \sin\theta d\theta \int_{-\infty}^{\infty} v_\omega D(\omega) d\omega \quad . \tag{27}$$

Taking the mode distribution function $D(\omega)$ to be slowly varying with respect to the spectrum width of the rf pulse, Δ^{-1}, and to $G_R(\omega)$ we obtain from Eqs. (17), (19), and (24)–(27)

$$V(t) = \frac{i\omega_0 aAD(0)m(d)B_0}{2\pi(1-i\beta)} \times \int_0^{2\pi} d\phi \int_0^\pi d\theta \Theta \sin\theta \cos\theta \times \int_{-\infty}^{\infty} d\omega S(t) G_R(\omega) \quad . \tag{28}$$

In the later discussion of the coherent nonlinear response of the sample consisting of a large number of particles we shall make use of Eq. (28) with $S(t)$ representing the solution to the appropriate nonlinear wave equations.

B. Dynamic polarization echoes in anharmonic oscillators

All echo phenomena are inherently nonlinear.[18–21] In order to pinpoint the echo formation mechanism it is necessary to have a model of the responsible nonlinearity. It has been clearly demonstrated[1,3] that the echoes in powders are due to the anharmonic interactions in oscillators but not due to the parametric field-mode interactions. In this section we review the model of the dynamic polarization echoes based upon the lattice anharmonicity.

The internal energy density U of a particle may be expressed by

$$U = U_L + U_{NL} \quad , \tag{29}$$

where the linear term U_L leads to the equation of motion for linear excitation of ionic motion, Eq. (18). We make a simplification retaining only the fourth-order lattice anharmonicity in the nonlinear term having the form

$$U_{NL} = (1/4!) c_4 \epsilon^4 \quad , \tag{30}$$

where $\epsilon \equiv \partial\xi(z,t)/\partial z$ is the strain and c_4 is an appropriate fourth-order elastic constant. The role of the third-order term causing harmonic generation and subsequent echo formation has been considered. It is noted that the results are similar to those obtained here from the fourth-order term.[1,22] Adding the force term coming from U_{NL}, $\partial^2 U_{NL}/\partial z^2$, to Eq. (18), the nonlinear wave equation is written by

$$\frac{\partial^2 \xi}{\partial t^2} + 2\Gamma \frac{\partial \xi}{\partial t} - v^2 \frac{\partial^2 \xi}{\partial z^2} - \frac{c_4}{2\rho} \left(\frac{\partial \xi}{\partial z} \right)^2 \frac{\partial^2 \xi}{\partial z^2} = \frac{B_0 B(t) \Theta \cos\theta}{4\pi\rho} \left(\frac{1+i}{\delta} \right) \times \left[\exp\left(\frac{-(1+i)(z+d)}{\delta} \right) - \exp\left(\frac{(1+i)(z-d)}{\delta} \right) \right] \quad . \tag{31}$$

The linear electromagnetic driving force on the rhs excites only those fundamental modes in the neighborhood of the applied rf frequency ω_0. We assume that for a given particle and frequency ω_0 only one such fundamental mode is excited. To lowest order of the fourth-order lattice anharmonicity, the nonlinear term on the left-hand side (lhs), causes nonlinear dispersion (amplitude dependent phase shift and damping) of the fundamental modes. Although the harmonic generation is allowed by the boundary conditions of a platelet, we neglect all harmonic generations. Assuming a solution to have the form given by Eq. (19a), we can rewrite Eq. (31) as

$$\frac{\partial^2 S}{\partial t^2}+2\Gamma\frac{\partial S}{\partial t}+\Omega^2(1+\mu|S|^2)S=\frac{\gamma B_0 B(t)\Theta\cos\theta}{4\pi\rho(1+\beta^2)^{1/2}}\ , \tag{32a}$$

where Ω^2 and γ are, respectively, given by Eqs. (20b) and (20c), and the nonlinearity constant μ is defined by

$$\mu=-\frac{3c_4}{2\rho\Omega^2}\int m\left(\frac{\partial m}{\partial z}\right)^2\frac{\partial^2 m}{\partial z^2}dV\Big/\int m^2 dV\ . \tag{32b}$$

1. Small-signal limit

We shall confine ourselves here to the case of the small-signal limit correct only to first order in the nonlinearity constant μ. In this case the nonlinearity can be neglected during the two applied pulses and after the first pulse. The solution [Eq. (22a)] of the equation for the linear excitation [Eq. (20a)] at the end of each applied pulse is used as the initial condition for the solution of the nonlinear equation represented by Eq. (32a) after the second pulse where $B(t)=0$. The exact solution of Eq. (32a) with $B(t)=0$ is given by

$$S(t)=S(t_0)\exp[(-\Gamma+i\Omega)(t-t_0)]\times\exp[i(\mu\Omega/4\Gamma)|S(t_0)|^2(1-e^{-2\Gamma(t-t_0)})]\ . \tag{33}$$

Here, the initial condition $S(t_0)$ at the trailing edge of the second pulse, $t_0=\tau+\Delta_2$, is given by applying Eqs. (22a)–(22c) to the linear excitation caused by applied two pulses, i.e., a superposition of the linear excitation by the first and second pulses. To first order in the nonlinearity constant μ, the solution of Eq. (32a) for the coherent response is given by

$$S(t)=(|\gamma|^2\gamma\mu\Omega/4\Gamma)\left[\frac{B_0\Theta\cos\theta}{8\pi\rho\Omega\Gamma(1+\beta^2)^{1/2}}\right]^3 B_1B_2^2e^{i\Omega(t-2\tau)}e^{-\Gamma t}(1-e^{-2\Gamma(t-\tau)})\left[\frac{e^{f^*\Gamma\Delta_1}-1}{f^*}\right]\left[\frac{e^{f\Gamma\Delta_2}-1}{f}\right]^2\ . \tag{34}$$

The output signal is obtained by inserting Eq. (34) into Eq. (28):

$$V(t)=\frac{i|\gamma|^2\gamma\mu e^{i\chi}aAD(0)m(d)B_1B_2^2B_0^4}{(8\pi\Gamma)^4\rho^3\Omega(1+\beta^2)^2}e^{i\omega_0(t-2\tau)}e^{-\Gamma t}(1-e^{-2\Gamma(t-\tau)})\times\int_0^{2\pi}d\phi\int_0^{\pi}d\theta\Theta^4\sin\theta\cos^4\theta\int_{-\infty}^{\infty}d\omega G_R(\omega)e^{-i\omega(t-2\tau)}\left[\frac{e^{f^*\Gamma\Delta_1}-1}{f^*}\right]\left[\frac{e^{f\Gamma\Delta_2}-1}{f}\right]^2\ . \tag{35}$$

Several significant properties can be noted in the small-signal limit. (i) The signal amplitude is proportional to the nonlinearity constant μ and increases with $B_1B_2^2$ and B_0^4. In the present model the excited modes, proportional to B_1B_0 and B_2B_0, couple anharmonically with each other to produce the coherent strain amplitude proportional to $(B_1B_0)(B_2B_0)^2$ as given by Eq. (34). The strain amplitude is detected electromagnetically in the static magnetic field as an echo signal proportional to $B_1B_2^2B_0^4$. On the other hand, in the parametric field-mode interaction model[1] the applied field of the second rf pulse parametrically couples to the previously excited modes (proportional to B_1B_0) to produce the coherent strain amplitude proportional to $B_1B_2^2B_0$. Accordingly, the resulting echo signal detected in the static field is proportional to $B_1B_2^2B_0^2$. (ii) The integral over all ω is nonzero only when $t\simeq 2\tau$. This is the coherent echo signal at $t\simeq 2\tau$. (iii) The echo amplitude builds up from zero at $\tau=0$ and has a maximum before decaying exponentially as $e^{-2\Gamma\tau}$ at $2\tau >> \Gamma^{-1}$. These properties will be compared to the experiment in Sec. IV.

Vadop'yanov *et al.*[12] have calculated the 2τ echo of the anharmonic oscillator system in which the individual oscillators are excited electromagnetically in the presence of the static magnetic field. They obtained that the echo amplitude varies with B_0^3, since they omitted the role of the static field B_0 in the detection of the echo signal. They also missed the buildup term, $(1-e^{-2\Gamma(t-\tau)})$, which comes from the integral of the nonlinear term $\mu|S|^2S$ in Eq. (32a) and is a characteristic property of the anharmonic oscillators.

2. *Large-signal regime*

In order to extend the small-signal result to arbitrarily large signals, we have to solve the full nonlinear inhomogeneous equation represented by Eq. (32a). However, the exact analytic solution is not available. Instead of a numerical integration of Eq. (32a) for a two-pulse sequence we evaluate analytically the anharmonic oscillator model by making an approximation in the following manner. Assuming that the pulse widths are short but finite so that the nonlinear term in Eq. (32a), $\mu|S|^2S$, can be neglected during the applied pulses, the solution during the pulses is given by Eq. (22a) which is used as the initial condition to the exact solution, Eq. (33), between and after the applied pulses. This approximation corresponds to that the nonlinearity is turned off during the short pulses. The expression for the voltage response corresponding to the echo which is nonzero near $t=m\tau$ $(m=2,3,4,\ \ldots\ )$ is given by

$$V(t)=i^m\frac{\gamma aAD(0)m(d)e^{i\chi}B_0^2}{16\pi^2\rho(1+\beta^2)}e^{-\Gamma(t-\tau)}e^{i\omega_0(t-m\tau)}$$

$$\times\int_0^{2\pi}d\phi\int_0^{\pi}d\theta\Theta^2\sin\theta\cos^2\theta\int_{-\infty}^{\infty}d\omega G_R(\omega)e^{-i\omega(t-m\tau)}e^{i\delta_m(\theta)}[e^{-\Gamma\tau}B_1\Delta_1g_1J_m(\eta)-iB_2\Delta_2g_2J_{m-1}(\eta)]\ , \tag{36a}$$

where

$$\delta_m(\theta)=\frac{\mu|\gamma|^2B_0^2\Theta^2\cos^2\theta}{2^8\pi^2\rho^2\Gamma\Omega(1+\beta^2)}\{B_1^2\Delta_1^2g_1^2[e^{-2\Gamma\tau}(1-e^{-2\Gamma(t-\tau)})-(m-1)(1-e^{-2\Gamma\tau})]+B_2^2\Delta_2^2g_2^2(1-e^{-2\Gamma(t-\tau)})\}\ ,$$

$$g_i=\sin(\omega\Delta_i/2)/(\omega\Delta_i/2)\ , \tag{36c}$$

$$\eta=\frac{\mu|\gamma|^2B_0^2\Theta^2\cos^2\theta}{2^7\pi^2\rho^2\Omega\Gamma(1+\beta^2)}B_1B_2\Delta_1\Delta_2g_1g_2e^{-\Gamma\tau}(1-e^{-2\Gamma(t-\tau)})\ . \tag{36d}$$

Here, $J_m(\eta)$ is the mth-order Bessel function of the first kind.

Multiple two-pulse echoes at $t=m\tau$ $(m=2,3,4,\ \ldots\ )$ arise naturally out of the anharmonic oscillator model as is noted in Ref. 1. Expanding Eq. (36a) to lowest order in η we find

$$V(t)\propto i^{m-1}\mu^{m-1}B_1^{m-1}B_2^mB_0^{2m}e^{-2\Gamma(t-\tau)}$$

$$\times(1-e^{-2\Gamma(t-\tau)})^{m-1}\ . \tag{37}$$

The $m\tau$ echoes decay as $e^{-2\Gamma(t-\tau)}$ at $2\Gamma(t-\tau)>>1$.

We shall discuss the transition from the small-signal limit represented by Eq. (35) to the large-signal regime confining ourselves to the case of $m=2$. It can be easily shown that Eq. (36a) reduces to Eq. (35) to lowest order in μ or η. In the large signal regime, however, the higher-order terms in η may contribute to the 2τ echo. Because of the nature of the Bessel function and the additional factor $e^{i\delta_m(\theta)}$ in Eq. (36a), one should expect both the B and τ dependence to be weaker at large η. Stokka and Fossheim[23] proposed an approximate analytic expression for the 2τ echo just above the low signal limit in accordance with the above argument. Their assumption is that the buildup and decay factors are given by $(1-e^{-2\Gamma\tau})^\nu$ and $e^{-(1+\nu)\Gamma\tau}$, respectively, with $\nu<1$. In the small-signal limit both factors reduce to those in Eq. (35) for $\nu=1$. Similar consistent modification can be brought about to the dependence on the rf and static magnetic fields and the prefactors

$$V(t)\propto(\mu\Omega/4\Gamma)^\nu(i\gamma^*B_1)^\nu(-i\gamma B_2)^{1+\nu}\left[\frac{\Theta\cos\theta}{8\pi\rho\Omega\Gamma(1+\beta^2)^{1/2}}\right]^{1+2\nu}B_0^{2(1+\nu)}e^{-(1+\nu)\Gamma\tau}(1-e^{-2\Gamma\tau})^\nu$$

$$\times\int_{-\infty}^{\infty}d\omega G_R(\omega)e^{-i\omega(t-2\tau)}\left[\frac{e^{f^*\Gamma\Delta_1}-1}{f^*}\right]\left[\frac{e^{f\Gamma\Delta_2}-1}{f}\right]^2\ . \tag{38}$$

In order to test whether or not the analytic expression is a good approximation to Eq. (36a) for the 2τ echo just above the low signal limit, we compare the 2τ dependence of the echo amplitude in Eq. (36a) obtained through numerical computation with that of Eq. (38) in Fig. 3. In Fig. 3 solid curves and closed circles represent Eqs. (36a) and (38), respectively. The comparison at several power levels shows that the approximate expression, Eq. (38), is quite appropriate in dealing with the large-signal effect except at the maximum power level, 20 dB. Here, 0 dB corresponds to the power level at which the central strain amplitude in the excitation spectrum at the trailing edge of each applied pulses is equal to

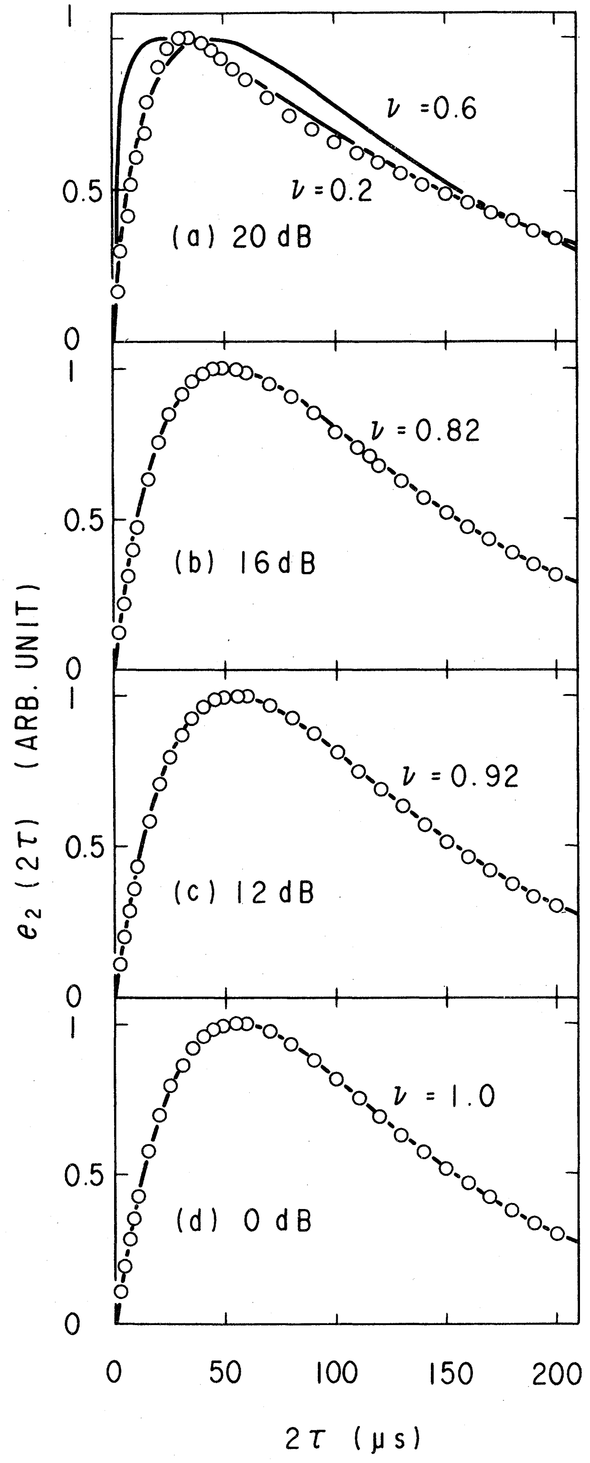

FIG. 3. (a)–(d) Comparison of the numerical computation of Eq. (36a) (open circles) with a conventional analytic formula for large-signal regime represented by Eq. (38) (solid curves). 0 dB corresponds to the power level at which the strain amplitude is 3×10^{-5}. The decay constant $\Gamma^{-1}=80$ μs is used.

3×10^{-5}. It is noted[24] that above the maximum power level shown in this figure, Eq. (36a) shows an oscillatory behavior against 2τ due to the nature of the Bessel function as observed in piezoelectric powders.[1,3,24]

It can be readily shown that three pulse echoes occur at $t=T+p\tau$ $(p=1,2,3,\ldots)$ for a three-pulse sequence when a similar procedure is repeated for the third pulse.

III. EXPERIMENTAL PROCEDURE

Metal powders of Al, Sn, Nb, and Cu used in the experiment were commercial ones and their purity ranged from 99.9% to 99.99%. All these powders were in the normal conducting state under the experimental condition described below. Type-II superconducting powder of V_3Si was obtained by grinding the bulk specimen which was prepared by arc melting of stoichiometric V and Si. All these specimens were washed and/or etched, and sized using standard mesh sieves. The sizes of the powder particles were chosen such that those particles had fundamental resonance frequencies of 15–45 MHz. Since even etched powder particles had irregular shapes, the mechanical vibration mode was considered to be very complex. The powder samples consisting of 10^5–10^6 particles were sealed, except for the case of measurements in He atmosphere, in Pyrex glass ampoules in a vacuum of 10^{-6} Torr after being outgased at 100 °C for Sn and at 400–500 °C for other powders for 20–30 h. The dimension of the glass ampoule was 1 cm in inner diameter and 2–3 cm in height.

A block diagram of the measuring circuits is shown in Fig. 4. rf pulses with carrier frequencies 10–100 MHz were applied to a sample with an rf coil. A variable capacitor was used to achieve the *LC* circuit resonance. The pulses were derived from two pulse generators (Matec 6600), whose relative pulse amplitudes, widths, and timing were independently adjusted. The maximum strength of the rf magnetic field was estimated to be 100 G.

Static magnetic fields were applied to the sample by using 45- and 125-kG superconducting magnets. Their field inhomogeneity in the sample was less than 1%. Most results were obtained at 4.2 K. Higher temperatures were obtained by controlling the current of a heater wound around the glass ampoule and measured with Au(0.03 at.% Fe)-Pt thermocouple attached to the bottom of the ampoule. In this case special care was taken to ensure thermal equilibrium of the sample and the thermometer.

IV. EXPERIMENTAL RESULTS

Two pulse echoes could be observed in powders of normal conducting Al, Sn, and Nb, and type-II su-

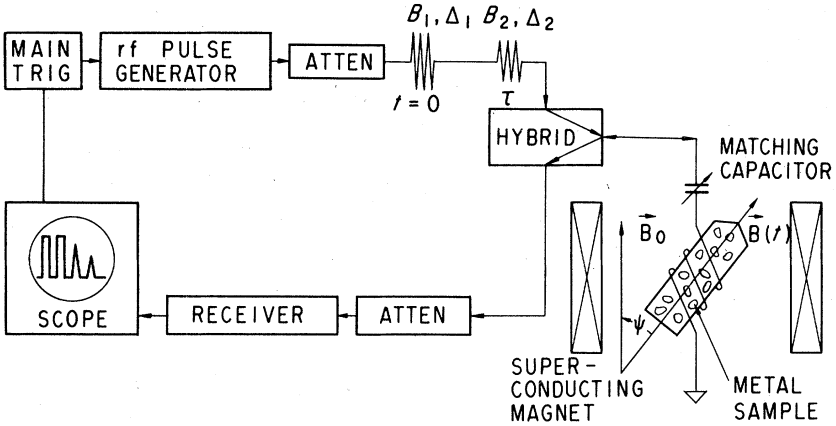

FIG. 4. A simplified block diagram for the echo measurements. The rf amplitudes B_1 and B_2, and the widths Δ_1 and Δ_2 of the two pulses are independently variable with two independent rf pulse generators and attenuators.

perconducting V_3Si in the mixed state. No echo in Cu powder was observed in static fields up to 45 kG, frequencies 10–45 MHz, and at 4.2 K. This results from the shape of the particles but not from the material itself. An etched Cu particle was observed with a microscope to be composed of several small particles sticking to each other firmly. In such a powder mechanical oscillation is strongly damped at the boundaries between sticking small particles and consequently no echo was formed. Pacult *et al.*[10] and Kupca and Searle[11] observed strong two-pulse echoes in good shaped Cu powders with the same order of dimensions as ours.

Weak three-pulse echoes were observed in Al, Sn, Nb, and V_3Si powders. The relationship $T_1 = \frac{1}{2} T_2$ was barely ensured only in Nb powders. Kupca and Searle[11] have reported the relationship holds for Al, Cu, and Ni powders at 4.2 and 77 K. In this paper we report two-pulse echoes only.

A. rf pulse interval dependence

The two-pulse echo amplitude $e_2(2\tau)$ as a function of twice the rf pulse separation, 2τ, is shown for Nb powder in Fig. 5. The buildup and decay behavior was observed in all materials measured in the present work. Dashed curve is the small-signal limit expected from Eq. (35) fitted to agree with experiment at the position where the echo amplitude has a maximum. As expected from the anharmonic oscillator model the echo amplitude builds up from zero at $\tau = 0$ and has a maximum before decreasing exponentially at large τ. The decay constant $T_2 = 1/\Gamma$ obtained from the data at large τ is 60 μs, whereas the dashed curve is obtained with $T_2 = 49$ μs. In general, the experimental results show that the buildup time constant is shorter and often much shorter than the decay time constant in contrast to the theory which predicts that both time constants are the same in the small-signal limit. This might be the reason why early workers did not notice seriously the nonmonotonic decay behavior, although brief description can be found in several literatures.[8, 11] The difference in buildup and decay time constants arises from at least two causes. (i) The powder sample is expected to be characterized by more than one value of decay constant Γ as discussed before,[1, 3] since the many different types of modes contributing to the echo have different Γ's. For small τ the modes with the largest Γ dominate which gives a fast buildup. The decay behavior for large τ is a measure of the Γ of the least damped modes. The dash-dot curve is obtained by

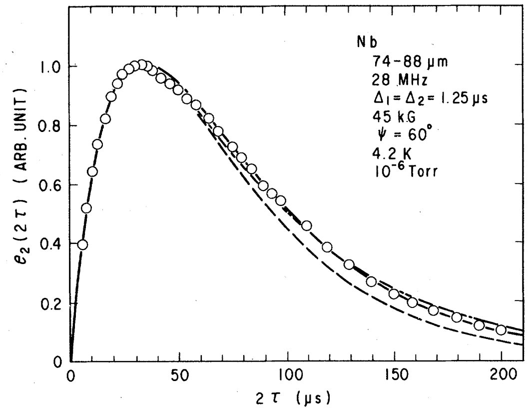

FIG. 5. Dependence of two-pulse echo amplitude $e_2(2\tau)$ on twice the pulse separation, 2τ, in Nb powder. The scale of the ordinate is arbitrary. The dashed curve corresponds to Eq. (35) fitted at the maximum of the echo amplitude. The dash-dot curve is obtained by assuming a Maxwellian distribution of Γ's, Eq. (39), and the small-signal limit. The solid curve corresponds to Eq. (38) fitted by varying Γ and ν.

assuming Maxwellian distribution of Γ's of the form

$$G_\Gamma(\Gamma)=[(\Gamma-\Gamma_c)/\Gamma_0]^2\exp\{-[(\Gamma-\Gamma_c)/\Gamma_0]^2/2\} \tag{39}$$

and the small signal limit with $\Gamma_0^{-1}=82$ μs and $\Gamma_c^{-1}=120$ μs. The fit is reasonably good within an experimental error. (ii) Another possible cause is a large-signal effect. As will be described in Secs. IV B and C the small-signal limit is quite difficult to obtain experimentally even in the lowest attainable rf power. The solid curve in Fig. 5 is obtained by fitting Eq. (38) to the data with $\Gamma^{-1}=53$ μs and $\nu=0.9$. Possible distribution in Γ and ν still remain in the large-signal regime as well. As will be shown in Sec. IV E different modes (transverse and longitudinal) contribute to the echo formation and therefore there is no reason to believe that they have the same Γ and/or ν.

In the large-signal regime multiple echoes, $e_2(m\tau)$, are observed at times $t=m\tau(m=3,4,\ldots)$ in addition to the echo at $t=2\tau$. The decay behavior of the 3τ echo in addition to the 2τ echo in Nb powder is shown as a function of $t-\tau$ in Fig. 6, where t is the time at which the echo is observed ($t=m\tau$). As expected from Eq. (37) the $m\tau$ echo decays as $e^{-2\Gamma(t-\tau)}$ when $2\Gamma(t-\tau)\gg 1$, where Γ is the same for all m.

The buildup and decay behaviors shown in Figs. 5 and 6 are the conclusive evidence for the anharmonic oscillator system.

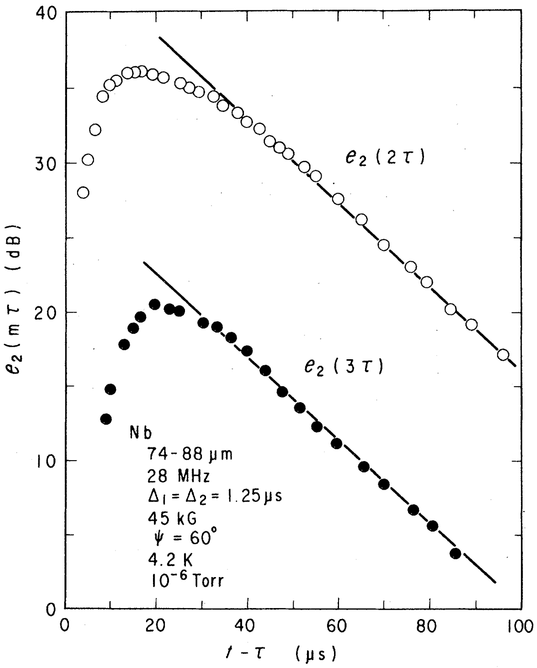

FIG. 6. Decay of the $m\tau$ echo amplitudes ($m=2,3$) in Nb powder plotted against $t-\tau$ (where $t=m\tau$).

B. rf pulse amplitude dependence

According to Eq. (35), when $B_1=B_2=B$ the 2τ echo amplitude should vary as B^3 in the small-signal limit. We show the rf power dependence obtained in Nb powder at a fixed τ in Fig. 7. In all the samples measured in the present study $e_2(2\tau)$ did not show B^3 dependence; i.e., the small-signal limit was not reached even at the lowest attainable rf power levels. We can expect from Eq. (38) that $e_2(2\tau)$ varies as $B_1^\nu B_2^{1+\nu}=B^{1+2\nu}$ when $B_1=B_2=B$ in the large-signal regime, where $\nu(\leq 1)$ is dependent upon the rf pulse amplitude. Fitting the data of Fig. 7 to $B^{1+2\nu}$ gives $0\lesssim\nu\lesssim 0.5$, whereas the analysis of the experiment on the τ dependence of $e_2(2\tau)$ gives $0.5\lesssim\nu\lesssim 0.9$ in the same power levels. A similar discrepancy can be seen in piezoelectric powders.[1,23] The discrepancy becomes small when the correction of the data taken at a constant τ is made taking into account that the factor $(1-e^{-2\Gamma\tau})^\nu e^{-(1+\nu)\Gamma\tau}$ is included in the echo amplitude, where ν is power dependent. The discrepancy also comes from the simplified expression of the echo amplitude for the large-signal regime. The expression in Eq. (38) is a good approximation to the results of numerical calculations only in a limited range of rf power levels as shown in Fig. 3. Furthermore, in the large-signal regime the theoretical predictions themselves of the anharmonic oscillator model become model dependent, although in the small-signal limit the predictions are unambiguous. Accordingly, in order to pinpoint the specific

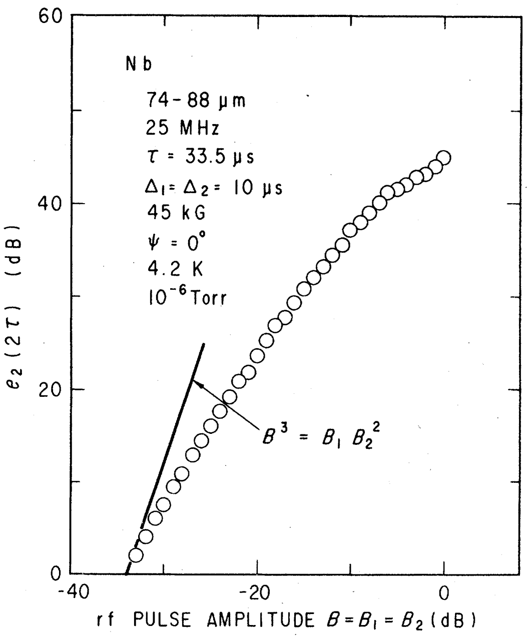

FIG. 7. Dependence of $e_2(2\tau)$ on rf pulse amplitude with $B=B_1=B_2$ for Nb powder. The straight line corresponds to B^3.

anharmonic oscillator model responsible for the echo formation mechanism it is necessary to observe the behavior in the large-signal limit. Piezoelectric powders exhibited a complex but internally consistent behavior of the large-signal limit.[1] The large-signal limit behavior was observed especially in the τ dependence of the echo amplitudes and their shapes in piezoelectric powders. Metallic powders exhibited the onset of large-signal behavior but not the transition to the large-signal limit.

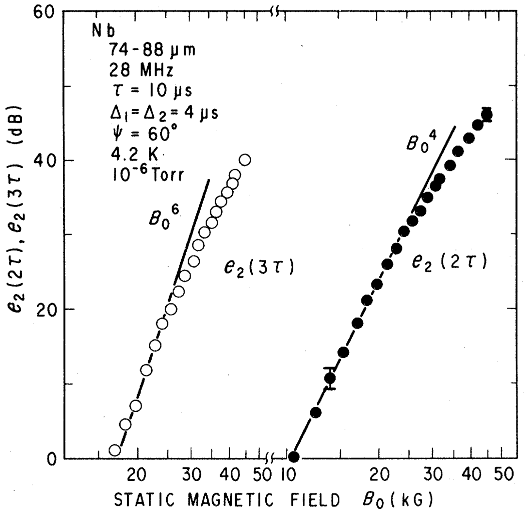

FIG. 8. Dependence of $e_2(2\tau)$ and $e_2(3\tau)$ on the static magnetic field B_0 for Nb powder. We take the minimum attainable signal level above the noise level as 0 dB for both $e_2(2\tau)$ and $e_2(3\tau)$. Therefore the relative magnitudes of $e_2(2\tau)$ and $e_2(3\tau)$ are not comparable with each other. The straight lines for $e_2(2\tau)$ and $e_2(3\tau)$, respectively, correspond to B_0^4 and B_0^6 expected from lowest order in the nonlinearity constant.

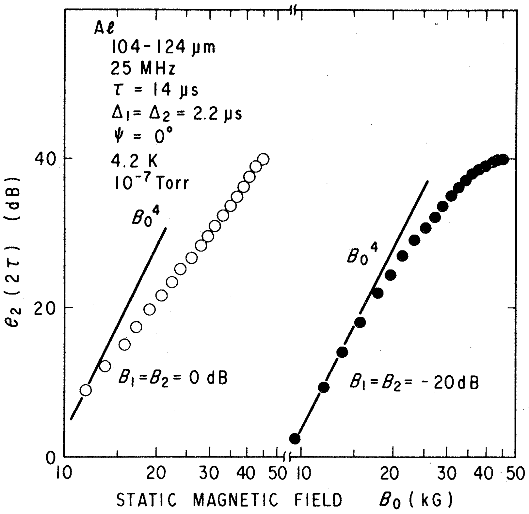

FIG. 9. Dependence of $e_2(2\tau)$ on B_0 for Al powder at different rf powder levels. 0 dB correspond to 10^2 G of the rf magnetic field amplitude. The straight lines of B_0^4 are expected from the small-signal limit.

C. Static magnetic field dependence

On the basis of Eq. (37) derived to lowest order in the nonlinearity constant μ, $e_2(2\tau)$ and $e_2(3\tau)$ should vary as B_0^4 and B_0^6, respectively, while in the parametric field-mode interaction model they should vary as B_0^2 and B_0^3, respectively. In the rf pulse amplitude dependence these two models are undistinguishable since both models give the same rf pulse amplitude dependence, e.g., $e_2(2\tau) \propto B_1B_2^2$, in the small-signal limit. In Fig. 8 we show B_0 dependence of $e_2(2\tau)$ and $e_2(3\tau)$ for Nb powder. From this figure we conclude that the anharmonic oscillator mechanism is responsible for the echo formation, although there are deviations from the expected small-signal behaviors at high static fields. Deviations from the small-signal behaviors are more clearly seen in Fig. 9, where the effect of rf pulse amplitude on the B_0 dependence is shown for Al powder. It was reported by Meredith *et al.*[17] that the amplitude of electromagnetically excited oscillation in Nb and Sn crystals were linearly dependent upon the static magnetic field up to 100 kG if corrected for absorption due to the static field. The amplitude could be large under the present resonance condition with high mechanical quality factors of the order of 10^4. We shall analyze the data by assuming the large-signal effect represented by Eq. (38) taking into account that Γ and ν are dependent upon B_0. In Fig. 10 we show $e_2(2\tau)$, e_{20}, Γ, and ν as a function of B_0 up to 120 kG. Here, the echo amplitude corrected for the damping, e_{20}, is obtained by extrapolating the τ dependence of $e_2(2\tau)$ at $2\Gamma\tau >> 1$ back to $\tau = 0$ and Γ and ν are obtained from the fitting of Eq. (38) to the τ dependence of $e_2(2\tau)$ obtained at various constant B_0's. The dependence of e_{20} [shown by open circles in Fig. 10(a)] on B_0 deviates from the small-signal behavior B_0^4 (shown by the solid line). The open circles in Fig. 10(b) show the damping constant Γ obtained from the fitting of Eq. (38) and the closed circles are the apparent damping constant Γ_A obtained at $2\Gamma_A\tau >> 1$. The two damping constants have the relationship

$$\Gamma = 2\Gamma_A/(1+\nu) \ . \tag{40}$$

The damping of mechanical oscillation caused by conduction electrons increases with B_0^2. The magnetic-field-independent background is due to mode conversion, phonon scattering, interaction with crystalline defects or impurities, etc., in particles. Measurements of the damping constant are discussed in Sec. IV F. The parameter ν shown in Fig. 10(c) is a mea-

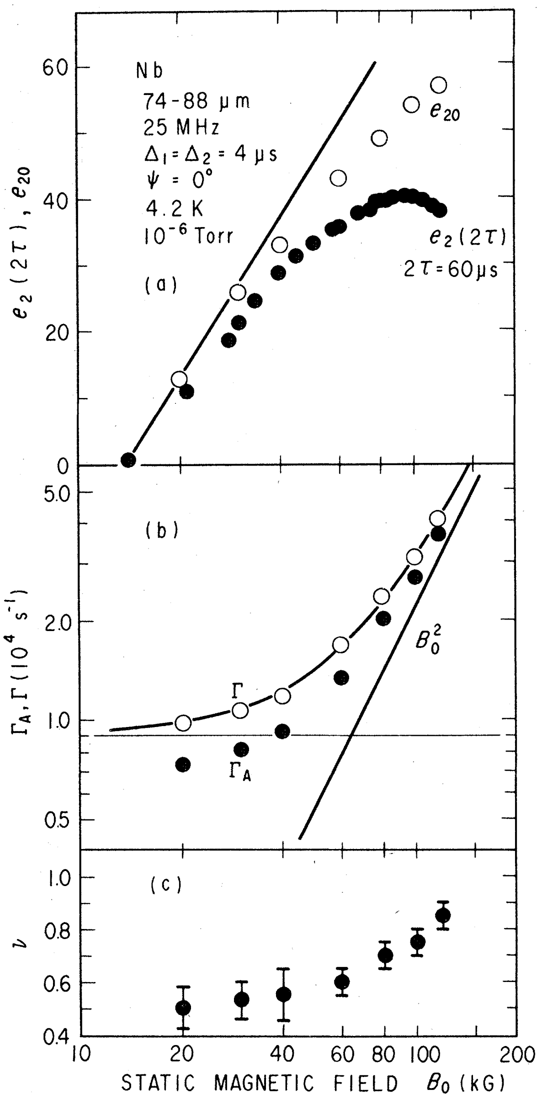

FIG. 10. (a) Dependence of $e_2(2\tau)$ and e_{20} on B_0. For determination of e_{20} see text. The straight line shows B_0^4. (b) Dependence of the decay constant Γ_A (closed circles) and Γ (open circles) on B_0. For determination of Γ_A and Γ see text. Solid curve is obtained by adding two parts [field-dependent ($\propto B_0^2$) and field-independent parts]. (c) Dependence of the large-signal parameter ν obtained from fitting Eq. (38) to $e_2(2\tau)$ data on B_0.

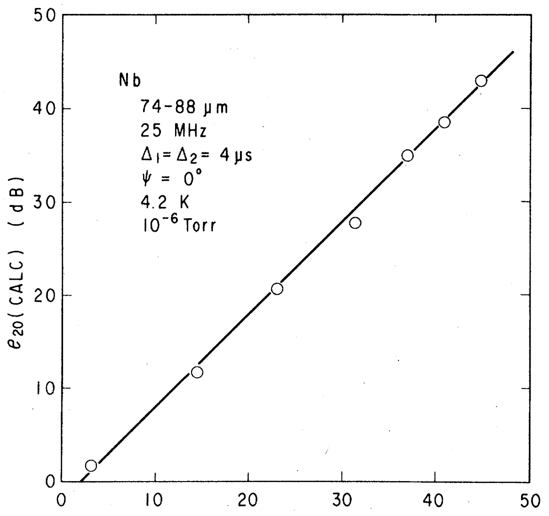

FIG. 11. Plot of Eq. (41) against experimental e_{20} on a log-log grid. The straight line shows a slope of 1.

sure of the large-signal effect. The increase of ν with increasing B_0 indicates that the large-signal effect is suppressed at higher fields. The oscillation amplitude is proportional to B_0/Γ as given by Eq. (22a). According to the result in Fig. 10(b) B_0/Γ tends to decrease at high fields and consequently the large-signal effect is suppressed. In order to examine whether or not the deviation of e_{20} in Fig. 10(a) from B_0^4 dependence is due to the large-signal effect, we compare in Fig. 11 e_{20} with the formula for the large-signal regime derived from Eq. (38)

$$e_{20}=\alpha[(3\pi^2/2^7)(c_4/c_2)\Omega]^{\nu}\times(B/4\pi\rho\Omega\Gamma d^2)^{1+2\nu}B_0^{2(1+\nu)}\ . \qquad (41)$$

Here, we used Γ and ν in Figs. 10(b) and 10(c), respectively, $c_4/c_2=100$,[25] $\Omega=(2\pi)25$ MHz, $B=100$ G, $\rho=8.6$ g/cm^3, and $d=40$ μm. The coefficient α includes the circuit response function and the constants which are comparatively insensitive to the static field dependent ν. The coefficient α does not appear explicitly in this figure where e_{20}(expt) and e_{20}(calc) are plotted in dB units (in a log-log grid). The linear relationship (slope 1 in Fig. 11) indicates that the echo amplitudes shown in Fig. 10(a) are consistently explained by Eqs. (38) or (41) with the large-signal-effect parameter ν and the damping constant Γ both of which are dependent upon the static magnetic field B_0.

Kupca and Searle[11] observed for all the samples they measured that $e_2(2\tau)\propto B_0^3$ and $e_2(2\tau)$ tends to saturate at high fields similarly to the closed circles in Fig. 10(a). They reserved the definite conclusion for the nonlinearity responsible for the echo formation, since the static field dependences deviated from the simple formulas, e.g., $e_2(2\tau)\propto B_0^4$, derived from the anharmonic oscillator theory in the lowest-order approximation, i.e., in the small-signal limit. Vodop'yanov *et al.*[12] obtained $e_2(2\tau)\propto B_0^3$ in their theoretical calculation. Although they obtained a good fitting to the data of Ref. 11 by taking into account of the B_0 dependence of Γ, they missed the role of the static magnetic field in the electromagnetic detection of the echoes. Since the strains due to echoes are detected through the static magnetic field as described in Sec. II, it is necessary to multiply by another B_0 in order to represent the detected echo signal amplitude.

In concluding the subsection the following can be noted: (i) The static magnetic field dependence definitely supports the anharmonic oscillator mechanism; and (ii) the deviation from the small-signal behavior in the static magnetic fields is consistently explained by the large-signal behavior expressed by Eq. (38) with the static field dependent ν and Γ.

D. Temperature dependence

On the basis of Eq. (35) the temperature dependence of the 2τ echo amplitude is determined by that of β represented by Eq. (1c) through σ_0 and that of Γ. Since the integral over ω in Eq. (35) gives a term proportional to Γ, it is expected that $e_{20}\Gamma^3$ is proportional to $(1+\beta^2)^{-2}$. The factor $(1+\beta^2)^{-1/2}$ is proportional to the electromagnetic excitation efficiency as given by Eq. (22a) and was obtained by Gaerttner *et al.*[26] for Al. In Fig. 12 we show $e_{20}\Gamma^3$ as a function of temperature. The solid curve for Al is obtained from the data of Gaerttner *et al.*[26] We do not have the information of Nb. We conclude that the temperature dependence of the echo amplitude is mainly determined by that of β and Γ. We shall discuss the temperature dependence of Γ in Sec. IV F.

E. Dependence on angle ψ between rf and static magnetic fields

It is shown in Sec. II that longitudinal- and transverse-acoustic waves can be produced depending on the orientation of B_0 relative to the shielding current at the metal suface. Although the geometry of the powders is complex compared to the specified surfaces of bulk specimens, we may obtain information on the oscillation modes excited in powders by varying the echo amplitudes with the angle between the directions of rf and static magnetic fields ψ. The excited oscillation mode has a longitudinal or transverse component when the value of Θ_x in Eq. (17b) or Θ_z in Eq. (17d) is not zero. When the thickness of the platelet corresponds to the resonance condition for the longitudinal mode, the dependence of the echo amplitude on the angle ψ when averaged over the distribution of θ and ϕ is given by

$$b_l(\psi) = \frac{1}{4\pi}\int_0^{2\pi} d\phi \int_0^{\pi} d\theta \Theta_x^4 \sin\theta \cos^4\theta$$

$$= \frac{1}{105}\sin^4\psi + \frac{2}{21}\sin^2\psi\cos^2\psi + \frac{1}{9}\cos^4\psi \ , \qquad (42a)$$

where we assumed uniform distribution of θ and ϕ, and only the fundamental mode oscillation. When the thickness of the platelet corresponds to the resonance condition for the transverse mode, the ψ dependence is given by

$$b_t(\psi) = \frac{1}{4\pi}\int_0^{2\pi} d\phi \int_0^{\pi} d\theta \Theta_z^4 \sin\theta \cos^4\theta$$

$$= \frac{1}{12}\sin^4\psi + \frac{4}{21}\sin^2\psi\cos^2\psi + \frac{8}{315}\cos^4\psi \ . \qquad (42b)$$

We assume that the detected echo consists of the longitudinal and transverse components

$$e_2(2\tau) = a_l b_l(\psi) + a_t b_t(\psi) \ , \qquad (43)$$

where coefficients a_l and a_t include excitation efficiency and particle numbers for longitudinal and transverse modes, respectively. In Fig. 13 we show $e_2(2\tau)$ as a function of ψ at 18 and 30 MHz for Nb powder. The dashed curve shows Eq. (43) with $a_l/a_t = 2.29$ for 18 MHz. The solid curve shows Eq.

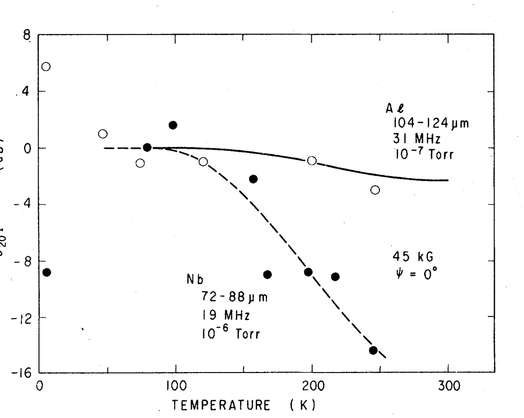

FIG. 12. Temperature dependence of $e_{20}\Gamma^3$. Solid curve for Al is obtained from Ref. 26. The dashed curve for Nb is drawn as a guide for the eye.

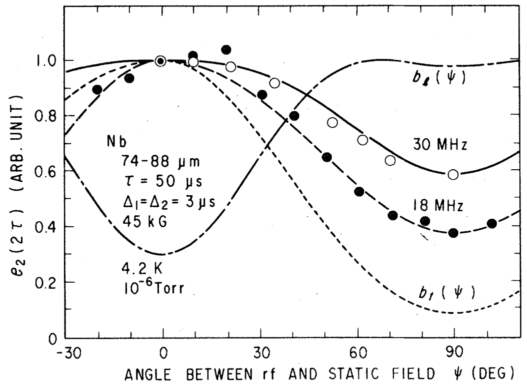

FIG. 13. Dependence of $e_2(2\tau)$ on the angle between rf and static magnetic field, ψ, for Nb powder at 18 (●) and 30 MHz (○). Dashed curve: Eq. (43) with $a_l/a_t = 2.29$. Solid curve: Eq. (43) with $a_l/a_t = 1.22$. Dash-dot curve: Eq. (42a). Dotted curve: Eq. (42b).

(43) with $a_l/a_t = 1.22$ for 30 MHz. The dash-dot and dotted curves, respectively, show $b_l(\psi)$ and $b_t(\psi)$. It is noted that the experimental results cannot be explained by only a single mode oscillation, $b_l(\psi)$ or $b_t(\psi)$. We conclude from this analysis that both longitudinal and transverse modes contribute to the echo signal. There is no reason to believe that only a single mode contributes to the echo formation in irregularly shaped powders.

F. Measurement of damping constant $\Gamma = T_2^{-1}$

The decay constant $\Gamma = T_2^{-1}$ of the two-pulse echoes is associated with decay of the amplitude of an individual oscillator whose energy decays as 2Γ. We assumed in the calculation presented in Sec. II that the particles are independent of each other and consequently there is no irreversible dephasing of particles. The assumption corresponds to the lifetime limited regime of conventional spin echoes ($T_2 = 2T_1$). We ensured that in Nb powders the decay time T_1 of the three-pulse echo is equal to $\frac{1}{2}T_2$ for dynamic echoes. Kupca and Searle[11] have found that the relationship $T_1 = \frac{1}{2}T_2$ holds for Al, Cu, and Ni powders at 4.2 and 77 K.

In this subsection we shall discuss the origin of the energy loss from a given mode of an individual oscillating particle. We have determined Γ from the decay of the two-pulse echo taking into account of the large-signal effect represented by Eq. (38). The oscillating energy is lost through internal frictions or through processes in which energy is transmitted through the surface of the particle to the surrounding medium. In the following discussion we shall see various experimental conditions which influence Γ.

1. *Effect of atmospheric pressure*

When the powders are immersed in gaseous medium the energy is lost through the surfaces. In Fig. 14 we show the damping constant Γ of Nb powder as a function of helium gas pressure at 26 and 36 MHz. The energy loss through the surface of the oscillating particle per unit time is given by

$$\frac{1}{U}\frac{dU}{dt} = -2\Gamma \ , \qquad (44)$$

where U is the energy of a given oscillation mode. The damping rate Γ is written as the sum of an intrinsic term, Γ_i, and a loss term of energy transmission from a particle to gas, Γ_g, i.e., $\Gamma = \Gamma_i + \Gamma_g$. The damping rate Γ_g can be expressed by using the acoustic impedances $Z_s(=\rho v)$ and Z_g of the solid and gas, respectively:

$$2\Gamma_g = (\omega_0/2\pi)[4Z_sZ_g/(Z_s+Z_g)^2] \simeq (2\omega_0 Z_g/\pi Z_s) \ , \qquad (45)$$

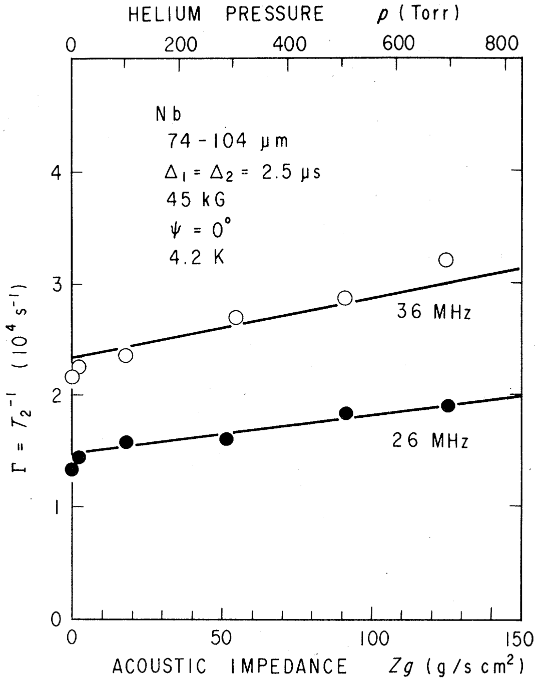

FIG. 14. Decay constant $\Gamma = T_2^{-1}$ as functions of acoustic independence Z_g and pressure p of He gas at 4.2 K in which Nb powder is immersed.

since $Z_s \gg Z_g$. The acoustic impedance of He gas, Z_g, at pressure p Torr is given by the product of the gas density, ρ_g, and the sound velocity, v_g,

$$Z_g = \rho_g v_g = (6.43\times10^{-2}p/T)(\tilde{\gamma}RT/M)^{1/2} = 0.183p\,(\mathrm{g/s\,cm^2}) \ , \qquad (46)$$

where $T = 4.2$ K is the temperature, $\tilde{\gamma} = 1.66$ is the ratio of the specific heat at constant pressure to that at constant volume for He gas, $R = 8.31\times10^7$ erg/mol deg is the gas constant, and $M = 4.0$ g is the molecular weight of He. From the slopes of the straight lines in Fig. 14 we obtain $Z_s \simeq 1.5\times10^6$ g/s cm^2 for Nb. Using $\rho = 8.6$ g/cm^3 we obtain an effective sound velocity $v \simeq 1.8\times10^5$ cm/s. This velocity is in good agreement with known velocities in Nb bulk material.[27] The intercept on the ordinate is a measure of the intrinsic loss rate Γ_i.

2. *Effect of frequency*

As indicated in Eq. (45) the energy loss to the He gas varies linearly with frequency, since the oscillation loses its energy every time it hits the particle surface. The intrinsic loss was measured in a vacuum. The frequency dependence of the intrinsic loss rate for Nb powder measured in a vacuum of 10^{-6} Torr is shown in Fig. 15. The intrinsic loss varies

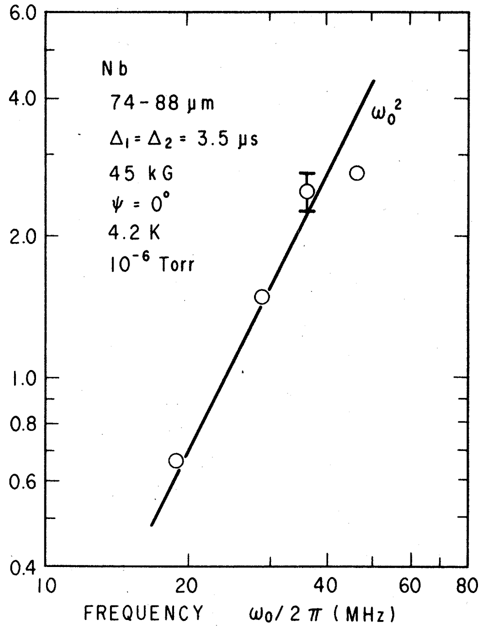

FIG. 15. Dependence of Γ on the carrier frequency $\omega_0/2\pi$ for Nb powder in vacuum. The solid line has a slope of 2.

with ω_0^2. Since theoretical predictions in Eqs. (11c) and (15c) indicate that the electronic loss varies with ω_0^2, we find from Fig. 15 that the nonelectronic loss Γ_0 in Eqs. (11b) and (15b) varies with ω_0^2 as well.

3. *Effect of static magnetic field*

The damping of sound vibration (acoustic attenuation) due to conduction electrons is affected by the static magnetic field as discussed in Sec. II A. Based upon Eqs. (11c) and (15c) the intrinsic loss due to the conduction electrons varies quadratically with the static field. In Fig. 10(b) we have shown the damping constant Γ with open circles for Nb powder as a function of B_0. The solid curve in Fig. 10(b) shows

$$\Gamma = \Gamma_0 + cB_0^2 \tag{47}$$

with $\Gamma_0 = 0.90 \times 10^4$ s^{-1} and $c = 2.2 \times 10^{-6}$ G^{-2}s^{-1} in fairly good agreement with the value calculated from Eq. (11c), 7×10^{-7} G^{-2}s^{-1}. The damping constant for type-II superconducting V$_3$Si powder is shown in Fig. 16. Since V$_3$Si has a lower critical field $H_{c1} \simeq 1$ kG and an upper critical field $H_{c2} \simeq 300$ kG at 4.2 K,[28] the magnetic flux density inside V$_3$Si powder under the present experimental condition with external field of 20–120 kG can be regarded as the same as that in vacuum, B_0. The experimental data of Γ shown in Fig. 16 are also expressed by Eq. (47) with $\Gamma_0 = 1.20 \times 10^3$ s^{-1} and $c = 3.08 \times 10^{-4}$ G^{-2}s^{-1}.

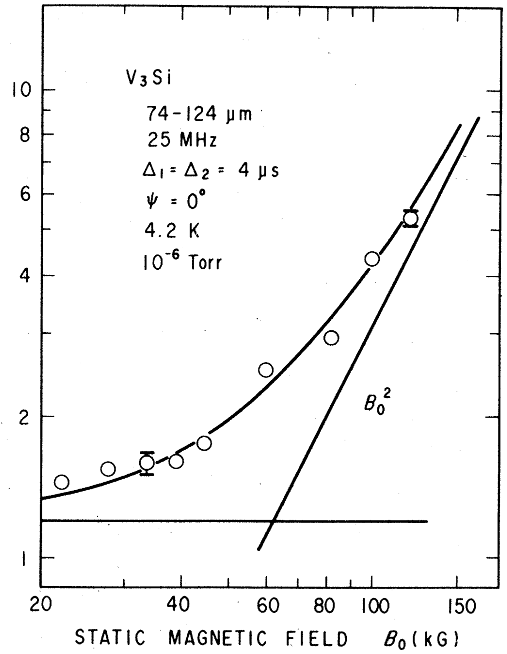

FIG. 16. Dependence of Γ on B_0 for V$_3$Si powder. Open circles are obtained by fitting the experimental data of $e_2(2\tau)$ to Eq. (38). Solid curve is the sum of the field-independent term, Γ_0, and the term which increases with B_0^2.

4. *Effect of temperature*

Temperature dependences of the damping constant for Al and Nb powders are shown in Fig. 17. The internal loss mechanisms consist of temperature-independent part, e.g., mode conversion, interaction with crystalline defects or impurities, and temperature-dependent part which is due to thermal

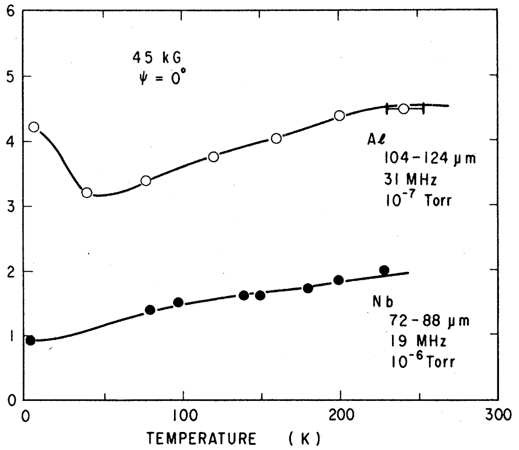

FIG. 17. Temperature dependence of the decay constant Γ for Al and Nb powders.

phonons and conduction electrons. Although the separation of these factors is outside the purpose of the present paper, the increase of Γ at low temperatures for Al may be related to the fact that the ultrasonic attenuation is proportional to the conductivity of metals.

We have shown the experimental results of the damping constant under various experimental conditions. The decay constant of the two-pulse echoes is associated with decay of the amplitude of an individual oscillator. The energy loss from a given mode of a particle is caused by internal loss due to mode conversion, interaction with crystalline imperfections, scattering of thermal phonons and conduction electrons, and by transmission of oscillating energy to the surrounding gas through the particle surface.

V. CONCLUSIONS

In Sec. II we have shown linear electromagnetic excitation of acoustic oscillation in a metal particle and formation of polarization echoes based on an anharmonic oscillation model both in the small-signal limit and in the large-signal regime. The dynamic polarization echoes observed in metallic powders have properties quite similar to those observed in piezoelectric powders at VHF range.[1,3] All the experimental results presented in Sec. IV showed that the polarization echoes in normal- and superconducting-metal powders are caused by an anharmonic oscillator mechanism but not by a parametric field-mode interaction mechanism. It was quite difficult to take data showing the small-signal limit behavior even at the lowest applied pulse amplitudes consistent with adequate signal to noise. Most of the data are in the large-signal regime and various factors which influence the echo formation are consistently explained by the calculation in the large-signal regime.

The main conclusions obtained from the present experimental study are summarized as follows: (i) The buildup and decay behaviors and the static magnetic field effect clearly showed that the echoes are caused by the anharmonic oscillator mechanism; (ii) rf and static magnetic field dependences of the echo amplitude are well explained by the large-signal behavior; (iii) temperature dependence of the echo amplitude is mainly determined by temperature-dependent damping constant and linear electromagnetic excitation efficiency; (iv) dependence of the echo amplitude on the angle between the directions of rf and static magnetic fields revealed that both longitudinal and transverse modes contribute to the echo signal and this is naturally expected for irregularly shaped powders; and (v) damping constant of the two-pulse echoes is associated with decay of the amplitude of an individual oscillator. The oscillating particle loses its energy through processes internal to the particle or through processes in which energy is transmitted to the surrounding gaseous medium. The internal loss mechanism includes mode conversion at the particle surface, interaction with crystalline imperfections, and scattering with thermal phonons and conduction electrons. Measurement made in He gas at various pressure is in good agreement with a calculation of the loss associated with the energy transmission between media of different acoustic impedances.

ACKNOWLEDGMENTS

The authors would like to acknowledge Professor T. Fukase for supplying us with V_3Si samples. One of the authors (F. T.) is indebted to Professor Y. Hiki and Dr. T. Ishiguro for having an opportunity to stay at the Electrotechnical Laboratory. The authors are grateful for discussions with Dr. T. Ishiguro, Dr. H. Tokumoto, Dr. K. Fossheim, Dr. R. L. Melcher, and Dr. N. S. Shiren.

---

[*] Permanent address: Faculty of Science, Tokyo Institute of Technology, Oh-okayama, Meguro-ku, Tokyo 152, Japan.

[1] For a detailed review of powder echoes and the distinction between parametric field-mode interaction system and anharmonic oscillator system, see K. Fossheim, K. Kajimura, T. G. Kazyaka, R. L. Melcher, and N. S. Shiren, Phys. Rev. B 17, 964 (1978).

[2] R. W. Gould, Phys. Lett. 19, 477 (1965).

[3] K. Kajimura, K. Fossheim, T. G. Kazyaka, R. L. Melcher, and N. S. Shiren, Phys. Rev. Lett. 37, 1151 (1976).

[4] F. Borsa and G. Bonera, Boll. Soc. Ital. Fiz. 50, 55 (1966).

[5] I. B. Goldberg, E. Ehrenfreund, and M. Weger, Phys. Rev. Lett. 20, 539 (1968).

[6] H. Alloul and C. Froidevaux, C. R. Acad. Sci. Ser. B 265, 881 (1967).

[7] H. Alloul and C. Froidevaux, Phys. Rev. Lett. 20, 1235 (1968).

[8] R. J. Snodgrass, Phys. Rev. Lett. 24, 864 (1970).

[9] E. Ehrenfreund, I. B. Goldberg, and M. Weger, J. Appl. Phys. 39, 5941 (1968).

[10] Z. A. Pacult, P. C. Riedi, and D. P. Tunstall, J. Phys. F 3, 1843 (1973).

[11] S. Kupca and C. W. Searle, Can. J. Phys. 53, 2622 (1975).

[12] B. P. Vodop'yanov, V. A. Zhikharev, and A. R. Kessel', Zh. Eksp. Teor. Fiz. 74, 185 (1978) [Sov. Phys. JETP 47, 94 (1978)].

[13] See also S. Kupca, I. Maartense, H. P. Kunkel, and C. W. Searle, Appl. Phys. Lett. 29, 224 (1976).

[14] For a review, see E. R. Dobbs, in *Physical Acoustics,* edited by W. P. Mason and R. N. Thurston (Academic, New

York, 1973), Vol. 10, p. 127.

[15] S. Rodriguez, Phys. Rev. 130, 1778 (1963).

[16] M. H. Cohen, M. J. Harrison, and W. A. Harrison, Phys. Rev. 117, 937 (1960).

[17] D. J. Meredith, R. J. Watts-Tobin, and E. R. Dobbs, J. Acoust. Soc. Am. 45, 1393 (1969).

[18] G. F. Herrmann and R. F. Whitmer, Phys. Rev. 143, 122 (1966).

[19] R. M. White, J. Appl. Phys. 37, 1693 (1966).

[20] W. H. Kegel and R. W. Gould, Phys. Lett. 19, 531 (1965).

[21] F. W. Crawford and R. S. Harp, J. Appl. Phys. 37, 4405 (1966).

[22] R. L. Melcher and K. Kajimura (private communication).

[23] S. Stokka and K. Fossheim, J. Phys. C 11, 3949 (1978).

[24] K. Kajimura, K. Fossheim, R. L. Melcher, and N. S. Shiren, The Sixth International Conference on Internal Friction and Ultrasonic Attenuation in Solids, Tokyo, 1977 (unpublished).

[25] See, for example, H. Soma and Y. Hiki, J. Phys. Soc. Jpn. 37, 544 (1974).

[26] M. R. Gaerttner, W. D. Wallace, and B. W. Maxfield, Phys. Rev. 184, 702 (1969).

[27] D. I. Bolef, J. Appl. Phys. 32, 100 (1961).

[28] T. Fukase, M. Tachiki, N. Toyota, and Y. Muto, Solid State Commun. 18, 505 (1976); Y. Muto, N. Toyota, K. Noto, K. Akutsu, M. Ishino, and T. Fukase, J. Low Temp. Phys. 34, 617 (1979); N. Toyota, T. Fukase, M. Tachiki, and Y. Muto, Phys. Rev. B 21, 1827 (1980).